Development of catalytic membranes over PdAu selective films for hydrogen production through the dry reforming of methane

Agustina Dalla Fontana, Betina Faroldi, Laura M. Cornaglia, Ana M. Tarditi*

Instituto de Investigaciones en Catálisis y Petroquímica, INCAPE, Universidad Nacional del Litoral, CONICET, Facultad de Ingeniería Química, Santiago del Estero 2829, 3000 Santa Fe, Argentina

ARTICLE INFO

ABSTRACT

PdAu composite membranes were applied in the preparation of catalytic membranes for hydrogen production. The APTES surface modification of PdAu membranes synthesized by sequential electroless deposition was carried out. Grafted samples were analyzed by means of XPS, SEM-EDS and DRIFT. XPS data showed that surface saturation was reached when a 0.5 v/v % of APTES was employed. The morphological study of the samples showed that after APTES functionalization a slightly change on the PdAu microstructure occurred. It was observed that the APTES-functionalized samples were stable after heating to 823 K for 2 h. In addition, these membranes retained their hydrogen permeability without detrimental effect over their selectivity. Catalytic Ru and Rh-based membranes were synthesized by the dip-coating method. The membranes were evaluated in the dry reforming of methane at 823 K. Even though only low conversions were obtained, these were slightly higher than those obtained for a fixed-bed reactor with the same amount of catalyst.

1. Introduction

The constant increase in the demand for electricity and heat has led to an intensification of fossil fuels utilization [1]. Developing clean energy has been commonly viewed as one of the most important steps to solve the problems of pollutant emission and climate change in the long run [2]. In this context, the use of hydrogen offers ways to minimize greenhouse emissions, reduce air pollution and diversify energy supply [3].

Concerning the production of high purity hydrogen, the application of membrane reactors (MRs) is favorable. In the MRs, hydrogen production and separation take place in the same vessel simultaneously [4]. Furthermore, these systems allow obtaining higher conversions compared to conventional processes. From this point of view, Pd-based membranes are a viable alternative to be applied in these processes bearing in mind their high selectivity towards hydrogen [5]. The dry reforming of methane (DRM) to produce synthesis gas ($H_2 + CO$) from CO_2 and CH_4 has gained increased interest in recent years due to the present requirement for the reduction of their emissions [6]. One disadvantage of the process is the low hydrogen yield due to the occurrence of the water gas shift reaction (WGS). To improve the reaction yield, palladium-based membrane reactors have been widely studied [7]. Gallucci and coworkers [8] reported a higher selectivity and lower coke formation using a Pd-membrane reactor in comparison with a conventional reactor. Cornaglia and coworkers [9] using a Pd tubular membrane packed with a Rh catalyst reported an equilibrium shift, with enhanced methane conversion at 773 K.

When hydrogen production is carried out in a MR, the catalyst is generally packed on the retentate side, where hydrogen diffuses across the catalytic bed towards the surface of the membrane. Due to the distance that exists between the catalyst and the selective film, a reduction in the hydrogen partial pressure towards the Pd membrane could take place. This can cause a concentration polarization gradient, leading to a decrease in the global yield of the process because the insufficient mass transport in the gas phase lowers the effective hydrogen partial pressure difference which consequently results in reduced hydrogen flux [10]. An alternative to solve this limitation is to use catalytic membranes (CMs), which would allow a more rapid and effective removal of the hydrogen across the membrane due to the direct contact between the catalyst and the selective film.

It has been reported that noble metal catalysts (Pt, Ru, Rh, Pd) are active for the DRM reaction, with high coke resistance and stability [6]. Within this group, the Rh supported catalyst presented the highest activity and stability, followed by ruthenium [6]. Ru shows itself as an interesting alternative because it presents a high resistance to coke formation and low cost [11]. Ru catalysts supported on mixed oxides of La_2O_3-SiO_2 have demonstrated to be active, stable for the DRM, and with high metal dispersion [12].

Concerning the use of catalytic membranes for hydrogen production, several reports in the literature apply them mainly for the water gas shift and methane steam reforming reactions [13–16]. However, as far as we know, a system of the type presented in this paper has not yet been proposed. We present a system based on a PdAu functionalized membrane, on which the catalyst was deposited on top of the alloy layer.

The goal of this work was to optimize the synthesis conditions of catalytic membranes, that will be used in a catalytic membrane reactor configuration, in which the active phase is deposited on top of the PdAu selective film. One of the most important things to considerer in order to improve the reaction yield is to ensure that an adequate amount of catalyst mass is deposited on the surface of the Pd-based membrane. The effect of the 3-aminopropyltriethoxysilane (APTES) functionalization of the PdAu surface, prior to the catalyst deposition, was evaluated and analyzed by XPS, SEM-EDS, and DRIFT. The CMs based on Ru and Rh catalysts were evaluated in the dry reforming of methane reaction to obtain high purity hydrogen and compare the performance with that of a fix bed reactor.

2. Experimental

2.1. Preparation of the PdAu membranes

As supports of the membranes, 0.1 μm grade porous stainless steel (PSS) 316 L discs (1.27 cm diameter × 2 mm thick) and non-porous stainless steel (NPSS) discs (1 cm diameter × 2 mm thick) were used. Before the metallic deposition, the supports were conditioned and modified as described elsewhere [17]. The alloy components of the membranes were deposited by means of sequential electroless plating deposition, using the bath compositions and conditions optimized in our previous publication [17]. After all the synthesis cycles finished, the samples were heated up to 773 K in flowing nitrogen. After that, the annealing process was conducted in hydrogen atmosphere applying a ΔP of 10 kPa to favor the metallic inter-diffusion and, consequently, the formation of the alloy.

2.1.1. Functionalization of the PdAu surface with APTES

For the optimization of the APTES (Merck 99%) concentration employed at the functionalization stage, PdAu films deposited on top of NPSS discs were used. Three different concentrations of APTES (0.1%, 0.5% and 1.0 v/v %) were evaluated, using anhydrous toluene as solvent. The PdAu membrane was submerged vertically inside a three-neck balloon flask, which contained the APTES solution. Nitrogen was bubbled on the solution under reflux and maintained for 1 h at 383 K. After this stage, the samples were dried in nitrogen atmosphere. An evaluation against a thermal treatment of a PdAu sample functionalized with a 0.5 v/v % APTES solution was carried out in a quartz reactor. The system was heated up to 823 K in inert flow at 1 K min^{-1} and was left at that temperature for 1 h. The morphological and compositional analyses of this sample were carried out before and after the treatment. The nomenclature used for the grafted samples was APTES(x)-NPSS, where x refers to the APTES solution concentration (v/v %).

2.2. Catalyst preparation

As catalysts, Ru and Rh solids supported on a binary La$_2$O$_3$(27%)-SiO$_2$ system were used. The support with 27 wt.% of La$_2$O$_3$ was prepared by incipient wetness impregnation of SiO$_2$ (Aerosil 200 calcined at 1173 K, average primary particle size 20–30 nm, specific surface area (BET) 200 ± 25 m^{2}g^{-1}) with lanthanum nitrate (Aldrich 99.9%), following the previously described procedure [12]. The subsequent incorporation of ruthenium or rhodium was also performed by incipient wetness impregnation, with RuCl$_3$.3H$_2$O (Alfa Aesar 99.9%) and RhCl$_3$·3H$_2$O (Alfa Aesar 99.9%) as precursor salts, followed by a drying step at 353 K. In the case of the Rh/La$_2$O$_3$-SiO$_2$ catalyst, the solid was

calcined at 823 K during 6 h. The nominal Ru and Rh loading was 0.6 wt.% for all catalysts, obtaining the following final composition: Ru(0.6%)/La$_2$O$_3$(27%)-SiO$_2$ and Rh(0.6%)/La$_2$O$_3$(27%)-SiO$_2$.

2.3. Preparation of the catalytic membranes

The catalyst was deposited on the surface of the APTES functionalized PdAu alloy by dip-coating from a 10 wt.% suspension of the catalyst in anhydrous ethanol at room temperature, followed by a drying step at the same temperature. The coating slurry pH was ~ 6. Eight or sixteen successive immersion-drying cycles were performed. In both cases, the disc was rotated 180 degrees after four immersion-drying cycles to improve the homogeneity of the catalyst deposition. After the last immersion-drying cycle, the samples were kept in a desiccator until their use.

2.3.1. Optimization of catalyst particle size

In order to optimize the size of the catalyst agglomerates and thus increase their dispersion on the PdAu membrane surface, the powder was sifted using two different sieves: 100 and 200 mesh. This allowed obtaining particles with a smaller size than 149 μm and 74 μm, respectively. The samples were modified with a 0.1 v/v % APTES, prior to the deposition of the catalyst and subjected to eight immersion-drying cycles at room temperature. Fig. 1 shows a simplified scheme of the steps followed to obtain a catalytic membrane. Table 1 shows the main characteristics of the samples studied.

2.4. Single gas permeation measurements of membranes

To evaluate the effect of APTES functionalization on the perm-selective properties, a PdAu membrane was evaluated before and after the APTES functionalization. For this purpose, the perm-selective properties were measured at 673 K and a ΔP of 50 kPa before and after thermal treatment. Single gas permeation measurements were carried out in a
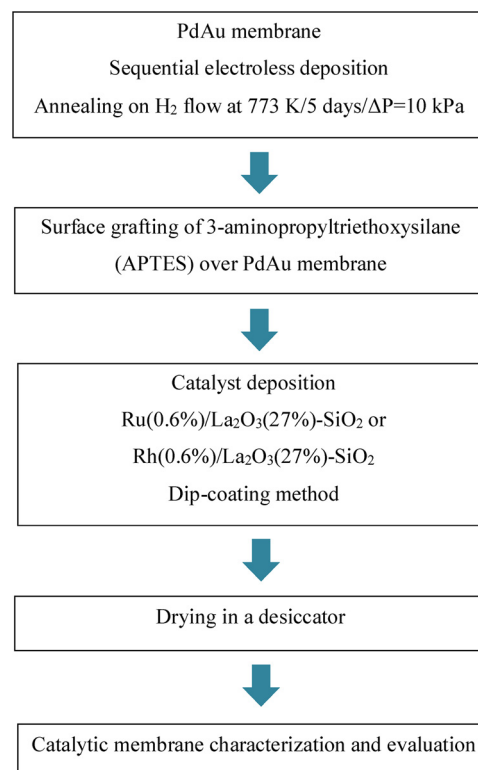

Fig. 1. Simplified scheme of the different steps to obtain the catalytic PdAu membranes.

A.D. Fontana et al.

Table 1
Samples studied in this work.

Sample	APTES concentration [v/v %]	Mesh	Thermal treatment[a]	Mass gain [mg][b]	Ethanol
Grafted membranes					
APTES (0.1%)-NPSS	0.1	–	No	–	No
APTES (0.5%)-NPSS	0.5	–	No	–	No
APTES (1.0%)-NPSS	1.0	–	No	–	No
Catalytic membranes					
CM1-PSS[c]	–	–	No	15.4	Yes
CM2-PSS[c]	0.1	–	No	7.0	Yes
CM3-PSS[c]	0.1	100	No	4.7	Yes
CM4-PSS[c]	0.1	200	No	0.6	Yes
CM7-PSS[c]	1.0	100	Yes	10.0	Yes
CM9-PSS[d]	1.0	100	No	9.0	Yes
Powder samples					
Ru-Fresh	–	–	No	–	No
Ru(Ar/573)	–	–	Yes	–	No
Ru-EtOH	–	–	No	–	Yes
Ru(Ar/573)-EtOH	–	100	Yes	–	Yes
Rh-Fresh	–	–	No	–	No
Rh-EtOH	–	–	No	–	Yes

[a] Thermal treatment of the catalyst in Ar flux at 573 K for 2 h prior to dispersion in anhydrous ethanol.

[b] Mass gain after deposition of the catalyst over the grafted membrane and drying at room temperature in a desiccator.

[c] Catalytic $Ru(0.6\%)/La_2O_3(27\%)$-SiO_2-based membrane.

[d] Catalytic $Rh(0.6\%)/La_2O_3(27\%)$-SiO_2-based membrane.

permeation device designed and built in our laboratory [18]. Using mass flow controllers, all gases were introduced into the permeator. The Pd alloy side of the membrane was in contact with the feed gases, while a N_2 sweep gas was used in the permeate side during the heating procedure. The effective permeation area of the membranes was ca. 0.5 cm^2 for half inch PSS discs.

2.5. Catalytic test

Measurements of catalytic activity were carried out using two different reactor configurations: fixed bed (FB) and catalytic membranes (CMs). For the evaluation of powder catalysts in a FB quartz reactor, the catalyst was diluted in ground quartz (size 70–40 mesh) to achieve adequate bed height, in this way avoiding canalizations in it. For the evaluation of the CMs, a stainless-steel reactor designed and built in our laboratory was employed. The sealing was reached by using graphite gaskets on both sides of the membranes.

Both systems were heated up to 823 K in inert flow at a speed of 1 K min^{-1}. Then, a reduction in hydrogen atmosphere was performed at this temperature for 2 h. After this step, the reaction mixture consisting of 32% CH_4, 32% CO_2 and 36% Ar v/v was fed to the reactor at 823 K. For the catalytic membrane evaluations, a sweep gas stream of 5 mL min^{-1} was used.

In order to analyze the influence of the metallic material used to construct the reactor-permeator on the conversion percentages, two measurements were made. In the first place, the evaluation was performed in the absence of the catalyst, heating the reactor-permeator to a heat up to 823 K in Ar flow. The second one was made by subjecting the permeator to an additional reduction in H_2 flow for 2 h at 823 K. These experiments showed negligible values for methane and carbon dioxide conversions. These results allowed us to discard the influence of

the material of the reactor over the conversions under the evaluated reaction conditions.

2.6. Samples characterization

The surface composition of the samples was determined by X-ray photoelectron spectroscopy (XPS). The XPS analyses were performed in a multi-technique system (SPECS) equipped with a dual Mg/Al X-rays source, and a hemispherical PHOIBOS 150 analyzer operating in the fixed analyzer transmission (FAT) mode. The spectra were obtained using a pass energy of 30 eV and the X-ray source was operated at 150 W and 11 kV. The working pressure in the main chamber was 5×10^{-10} kPa. For the quantitative analysis, the regions corresponding to Pd 3d, Au 4f, C 1s, O 1s, Na 1s, Si 2p and N 1s core levels were recorded for each sample. The data treatment was performed with the Casa XPS program (Casa Software Ltd, UK). The peak areas were determined by integration employing a Shirley-type background, the peaks being considered a mixture of Gaussian and Lorentzian functions. For the quantification of the different elements, sensitivity factors provided by the manufacturer were employed.

The bulk composition of the samples was analyzed by X-ray fluorescence (XRF). The measurements were performed using an EDX-720 Shimadzu X-ray Fluorescence Spectrophotometer with a 50-kV tube voltage, a Mo/Ni filter and a 5-mm collimator. A sample holder with a 5 μm thick polypropylene film and air atmosphere were used. The quantification was performed by the calibration curve method, for which reference samples of known composition were prepared by the same method of synthesis as the samples under study. The integration time was 200 s, and for the quantification emission lines Ru Kβ, Rh Kα, La Lα and Si Kα were considered.

Images of the outer surfaces and cross-sections of the samples were obtained using a JEOL scanning electron microscope model JSM-35 C. EDS analyses were performed employing a Phenom ProX scanning electron microscope (SEM) in order to determine the bulk atomic composition of the membranes.

To study the APTES anchorage on the PdAu membrane surface, the samples were analyzed by DRIFT spectra using a Shimadzu IRPrestige-21 spectrophotometer.

3. Results and discussion

3.1. Optimization of the APTES functionalization on PdAu surfaces

After metal depositions, the PdAu membranes were subjected to a heat treatment at 773 K in hydrogen flow. In all cases the complete alloy formation was observed in its fcc phase. In agreement with our previous report, the synthesized membranes had a volumetric gold atomic composition of ca. 5% and a thickness of ~14 μm [17].

With the aim to prepare catalytic PdAu-based membranes, different synthesis parameters were investigated: i) the functionalization of the PdAu alloy with APTES to improve the catalyst adhesion and ii) the catalyst particle size to improve the dispersion over the alloy surface.

In order to confirm the synthesis route for the catalytic membranes via APTES functionalization and optimize the employed APTES concentration, the APTES(0.1%)-NPSS, APTES(0.5%)-NPSS and APTES (1.0%)-NPSS samples were prepared and characterized by XPS. Fig. 2 presents the N 1s spectra of the analyzed samples. In all cases, after APTES grafting on the surface, two N 1s peaks located at 399.1 eV and 401.1 eV were detected, which could be assigned to the different anchorage modes of APTES (direct silane coupling or reverse coupling through the terminal amine group). The anchorage of the APTES molecule could be produced by covalent bonding between the oxide or hydroxyl groups at the surface, formed as a result of PdAu exposure to the environment, with the terminal silanol group of the APTES molecule. However, hydroxyl groups on the surface can either react with the Si end of APTES to form a silanized surface or with the amine group. If
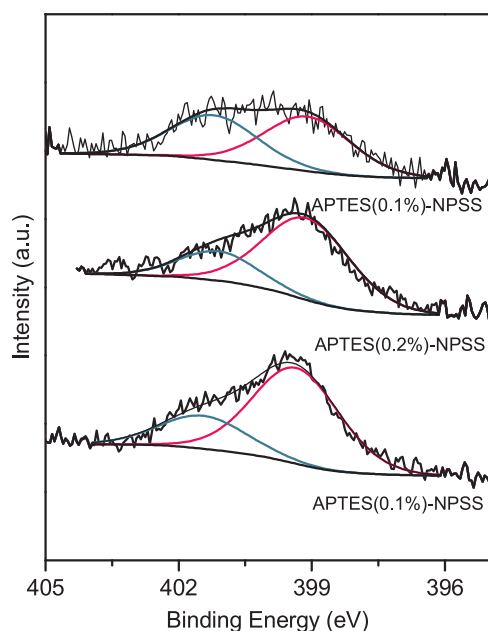
Fig. 2. N 1s spectra of the APTES(0.1%)-NPSS, APTES(0.5%)-NPSS and APTES (1.0%)-NPSS samples.

Fig. 4. DRIFT spectra of the APTES(0.1%)-NPSS sample after APTES functionalization.

the coupling process takes place via any of the hydroxyls of the silane, the free NH$_2$ termination is observed at 399.4 eV. On the other hand, if reverse attachment occurs, this leads to the appearance of a N 1s peak at 400.9 eV [19,20]. In addition, this peak could also be assigned to protonated amines species [19]. In our case, the two signals were observed in all the samples, with a higher contribution of the peak located at lower binding energy (~399.1 eV) for the samples synthesized employing 0.5% and a 1.0 v/v % of APTES (Fig. 2). It is noteworthy that the presence of silicon could suggest a correct grafting because this element was not present at the surface of unmodified PdAu samples (Si 2p spectra not shown). For this reason, the Si/Pd ratio is a good quantitative measure to evaluate the proportion of APTES anchored to the surface, as shown in the paragraph below. Both Pd and Au signals showed, as expected, a decrease in their intensity after grafting (spectra not show).

Fig. 3 shows the Si/Pd, N/Pd and Si/(Pd + Au) surface and volumetric atomic ratios of the PdAu membranes as a function of the APTES concentration used during the grafting procedure, determined by means
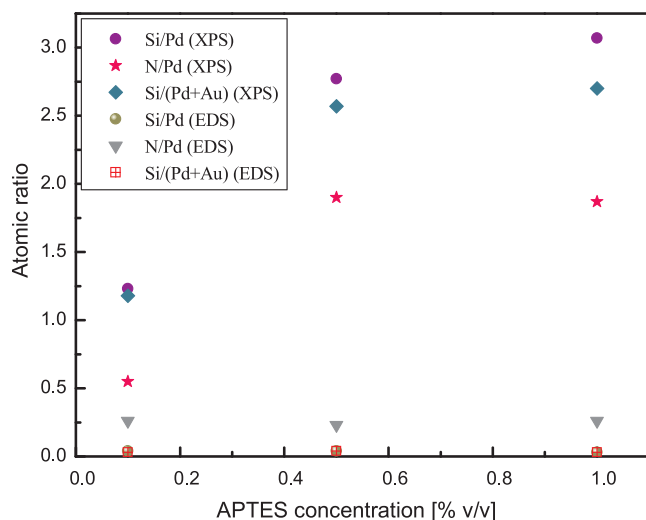

Fig. 3. Variation of the surface and volumetric atomic ratios as a function of the APTES concentration employed at the functionalization stage.
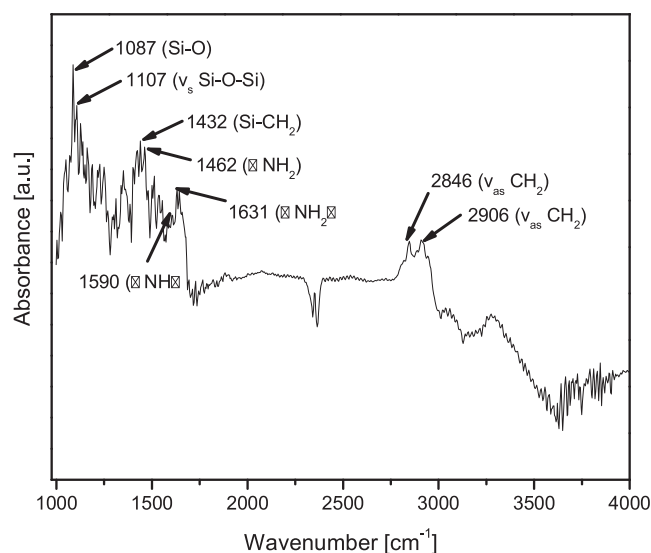
of XPS and EDS, respectively. The reported composition is an average value of the data obtained for each sample. It is clear from the curve that the increase of the APTES concentration led to an increase in the Si/Pd and N/Pd surface ratio. Furthermore, the obtained results suggest that upon using a 0.5 v/v % APTES solution, a surface saturation was reached (Fig. 3). For a PdAu unmodified membrane, a N/Pd surface ratio of 0.13 was determined. This value was lower than that obtained for PdAu functionalized membranes. The nitrogen detected in the non-functionalized sample probably comes as a residue of the EDTA employed at the synthesis bath. Nevertheless, note that the Si/Pd surface ratio is higher than the N/Pd ratio for all the samples. Regarding the Si/Pd and N/Pd volumetric ratio, it can be observed that these show similar values for all the evaluated samples (Fig. 3). The theoretical N/Si atomic ratio on APTES molecule is 1, and the experimental ratios were 0.44, 0.68 and 0.65, for the APTES(0.1%)-NPSS, APTES(0.5%)-NPSS and APTES(1.0%)-NPSS samples, respectively.

Grafted samples were also analyzed by DRIFT to verify the anchoring of APTES to the PdAu surface (Fig. 4). It should be noted that although the presented spectrum corresponds to the APTES(0.1%)-NPSS sample, the same bands were observed in all the evaluated samples. The spectrum corresponding to the APTES(0.1%)-NPSS sample contains bands at 1107 cm^{-1}, 1087 cm^{-1}, and 1432 cm^{-1}, which could be attributed to the Si−O−Si symmetric stretching vibration [21], the Si−O stretching vibration [22] and the deformation mode of the Si−CH$_2$ [23], respectively. The characteristic asymmetric stretching vibration of the CH$_2$ groups of the propyl chain of the silylating agent [24] can be observed at 2846 cm^{-1} and 2906 cm^{-1}. This typical vibration confirms the grafting of the amine onto the surface [25]. The peaks located at 1590 cm^{-1}, 1631 cm^{-1} and 1462 cm^{-1} are assigned to the characteristic asymmetric N−H bending (ν(NH$_2$)) and the NH$_2$ symmetric bending vibrations, respectively.

When the morphology of the functionalized samples is analyzed, a different structure can be seen throughout the surface, compared to the membrane without APTES (Fig. 5a and b). To the best of our knowledge, the formation of characteristic structures after the surface modification of PdAu alloys with APTES has not been yet reported in the literature. With the increasing APTES concentration, a change in the surface morphology is observed. In the case of the APTES(0.1%)-NPSS sample (Fig. 5c and d), the formation of finger-like structures on the surface is clearly seen. On the other hand, the APTES(1.0%)-NPSS sample presented a more pronounced change in the morphology (Fig. 5e and f). With the purpose of analyzing the elemental distribution
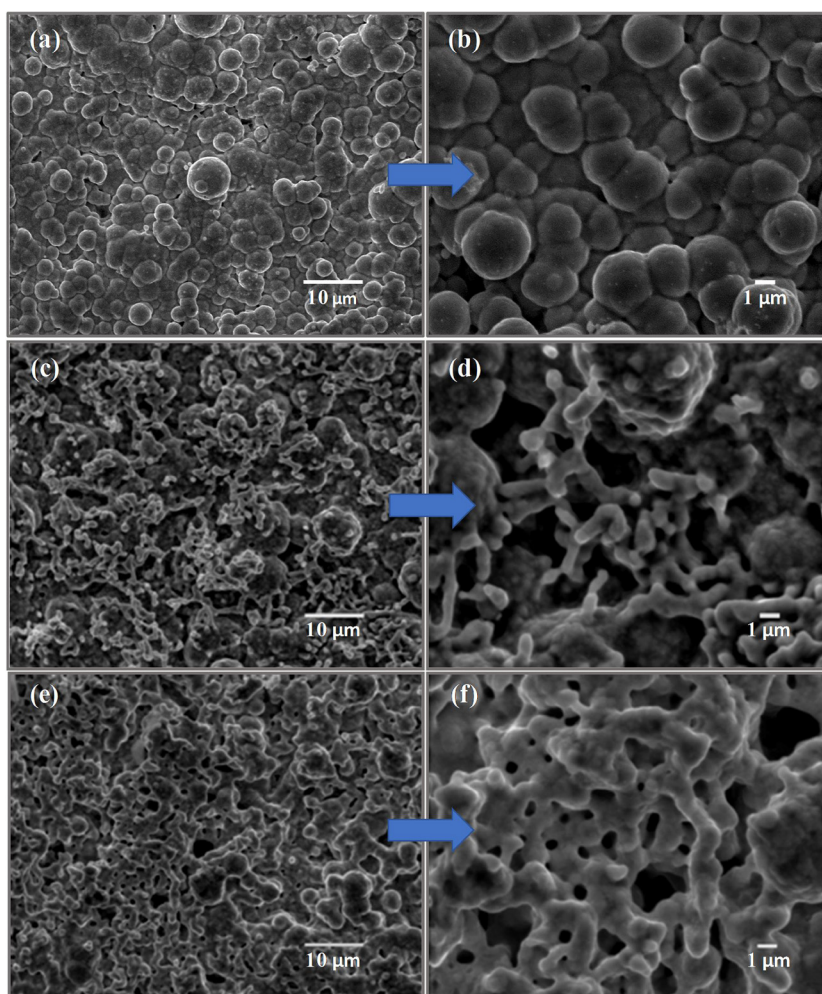
A.D. Fontana et al.

Fig. 5. Surface modification of the PdAu membranes before (a, b) and after the use of a 0.1v/v % APTES solution (c, d) and a 1.0v/v % APTES solution (e, f).

Table 2
Volumetric composition determined by EDS for the APTES(0.1%)-NPSS, APTES(0.5%)-NPSS and APTES(1.0%)-NPSS samples.

Sample	Atomic composition (at. %)			
	Pd	Au	Si	N
APTES(0.1%)-NPSS				
Zone 1	65.9	13.1	2.5	18.5
Zone 2	67.6	10.8	2.3	19.3
Zone 3	66.6	15.7	2.6	15.1
APTES(0.5%)-NPSS				
Zone 1	73.5	3.0	3.2	20.3
Zone 2	72.3	10.4	2.7	14.6
Zone 3	74.0	7.4	2.6	16.1
Zone 4	72.9	6.9	2.9	17.2
APTES(1.0%)-NPSS				
Zone 1	73.3	6.1	2.5	18.1
Zone 2	73.7	5.9	3.4	16.8
Zone 3	68.3	7.7	4.6	19.4
Zone 4	70.7	7.5	2.7	19.1

on top of the functionalized alloys, EDS scans were carried out on three (APTES(0.1%)-NPSS) and four (APTES(0.5%)-NPSS and APTES(1.0%)-NPSS) different zones. It is important to note that the reported values for each zone were obtained as a mean of different points. Table 2 summarizes the atomic composition determined at the different zones of the samples. It is important to note the existence of a uniform distribution of Pd, N and Si for all the samples, which was observed after

APTES functionalization at 383 K.

Since the catalytic membranes will be used in catalytic reforming reactions at high temperatures, the thermal stability of the APTES functionalized samples was studied. With that purpose, we studied the surface of a PdAu membrane with 1.0 v/v % of APTES before and after thermal treatment in Ar stream at 823 K. SEM surface images corresponding to the modified membrane are shown in Fig. 6. Clearly, no visible changes were observed in the morphology of the functionalized binary membrane after thermal treatment at 823 K (Fig. 6c and d).

Parallel to the morphological analysis performed by SEM, the volumetric and surface composition of the APTES-functionalized sample, before and after treatment at 823 K during 2 h, was analyzed by XPS and EDS. After treatment, a N/Pd volumetric ratio equal to 0.4 was determined. This ratio was very similar to that reported for the modified unheated sample.

Chen et al. [26] investigated the effect upon the mechanical and thermal properties of functionalized reduced graphene oxide when it was introduced to composite with poly(styrene-co-maleic anhydride). They found that the mechanical properties and heat stability of the composites were largely increased in the high temperature region (573–873 K). They also showed that a 0.2 wt.% addition of functionalized reduced graphene dramatically increased the storage modulus of poly(styrene-co-maleic anhydride) in the high temperature region by one order of magnitude compared with neat poly(styrene-co-maleic anhydride).
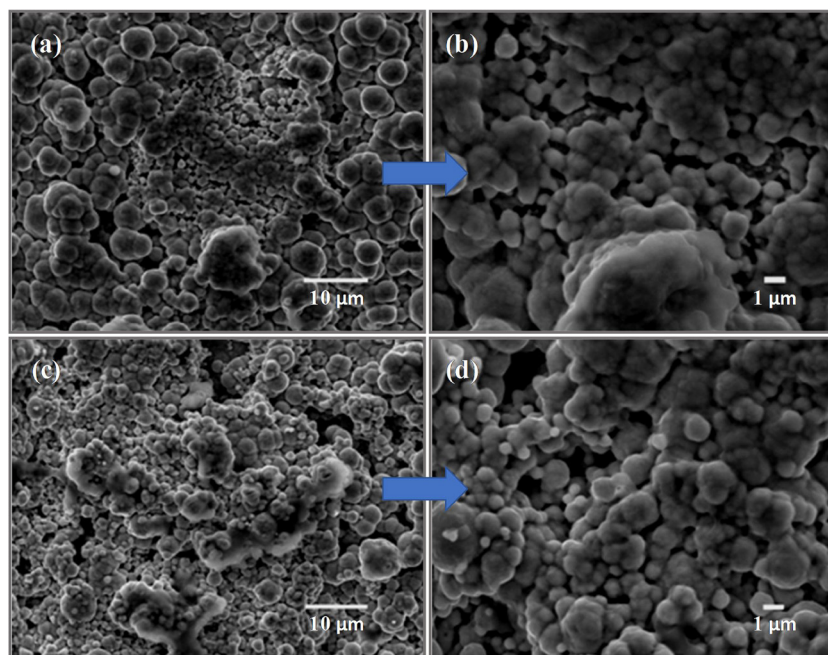
Fig. 6. PdAu functionalized membrane before (a, b) and after (c, d) thermal treatment at 823 K.

3.2. Effect of the APTES functionalization on the permeability of the PdAu membranes

The mechanism of hydrogen permeation through dense metal membranes has been extensively studied [8]. As proposed by Lewis [27] in his pioneering work, the hydrogen transport mechanism through Pd-based membranes involves several stages including mass transfer to the membrane surface, dissociation-adsorption on the alloy surface and bulk diffusion of hydrogen into the bulk. It is important to note that depending on factors such as membrane thickness, surface roughness, selectivity and gas purity, the rate controlling step for H_2 permeation could be different [28]. Due to the existence of this transport mechanism, the APTES surface modification employed in our case should not modify the characteristics of the PdAu membrane to ensure that it continues to maintain its perm-selective properties.

Under the conditions described in the experimental section, the perm-selective properties of a PdAu membrane before and after the functionalization were evaluated. The membrane presented a hydrogen permeability of 1.2×10^{-8} mol m $s^{-1} m^{-2} Pa^{-0.5}$ before APTES grafting and of 1.1×10^{-8} mol m $s^{-1} m^{-2} Pa^{-0.5}$ after that procedure. This value is in the range of the one reported for membranes of these characteristics, which includes values between $0.9–1.3 \times 10^{-8}$ mol m $s^{-1} m^{-2} Pa^{-0.5}$ at 673 K and 50 kPa [17]. Nitrogen flow was not detected, indicating that the membrane is composed of a continuous film free of cracks. This also indicates that PdAu functionalized membrane retains its perm-selective properties after the surface modification with APTES. The results obtained show that the use of APTES for the surface modification of PdAu membranes does not modify their hydrogen permeation and selective properties.

3.3. Deposition of the catalyst on the PdAu composite membranes

The CM1-PSS sample was obtained by successive immersions of the as prepared Ru-catalyst on the surface of the PdAu membrane, after the alloy formation and without previous APTES functionalization. In this case, ten successive immersions followed by drying at room temperature were performed. Although the mass gain after drying at 353 K was about 15 mg (Table 1), the coating of the deposited catalyst was not stable after its reduction at 823 K for 2 h. This process was corroborated

by the loss of mass. Considering this observation, and in order to increase the adhesion and stability of the catalyst on top of the membrane, a synthesis route which included APTES surface functionalization of the PdAu surface was performed. When APTES was employed to modify the PdAu surface, the terminal amino group ($-NH_2$) of the molecule was hydrolyzed and then, it could be linked to the catalyst facilitating its anchoring to the surface of the membrane. For this reason, it is desirable to obtain surface amine groups over the grafted samples. The CM2-PSS membrane, which was functionalized with APTES prior to the catalyst deposition, was stable after heating in Ar flux at 823 K with a change of the catalyst mass lower than 10% after treatment. The use of APTES to increase or promote adhesion during the synthesis of different materials has been reported in the literature. Caro and coworkers [29] developed a synthesis route to improve the zeolite [29] and ZIF-90 [30] films deposition by chemically modifying the supports with APTES as a covalent linker at 383 K for 1 and 2 h, respectively. The authors reported the use of 3-aminopropylsilyl groups as an efficient molecular linker to attract and anchor the zeolite or ZIF nutrients onto the support surface during the hydrothermal synthesis at 333 K/24 h and at 373 K/18 h, respectively. In a previous work [31], we have shown an improvement in the morphology and stability of the zeolite NaA membranes synthesized on top of APTES modified porous stainless steel substrates after evaluation at 473 K. The hydrogen permeation flux through the membranes deposited on top of APTES-modified substrates remained stable after 10 days.

Fig. 7 shows the morphology of the Ru-based catalytic membranes. Based on the SEM analyses from different zones of the CM2-PSS membrane, a homogeneous distribution of the catalyst on the surface can be observed (Fig. 7a and b). While the coverage of the catalyst on the surface is homogeneous, there appear certain agglomerates of particles of the solid. In order to homogenize the size of these agglomerates and increase the dispersion of the catalyst on the surface of the PdAu membranes, the solid was sieved before dispersing it in anhydrous ethanol. CM3-PSS and CM4-PSS membranes were prepared employing powder catalyst with a particle size smaller than 149 μm and 74 μm, respectively. Fig. 7 also shows the SEM images of the CM3-PSS (Fig. 7c and d) and CM4-PSS (Fig. 7e and f) samples after reduction at 823 K in H_2 flux for 2 h. From the morphological analysis of the studied membranes, a greater coverage on the CM3-PSS sample can be
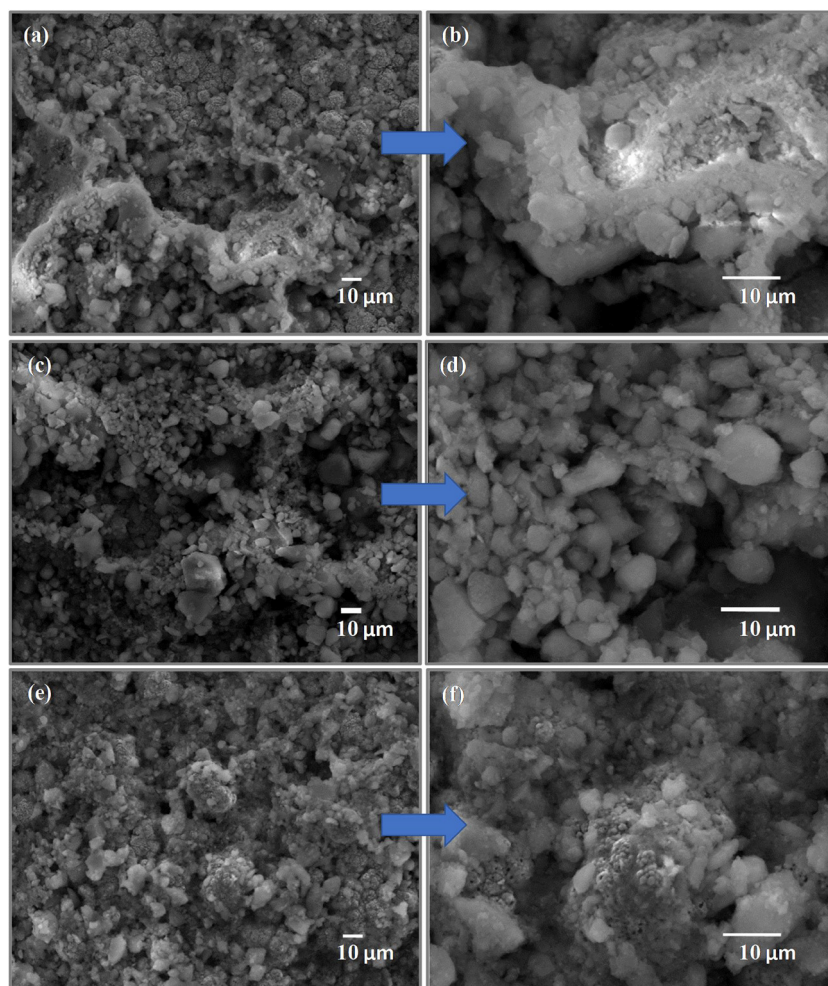
Fig. 7. Effect of the catalyst sifting on the surface coverage: CM2-PSS without sifting (a, b), CM3-PSS sifting with 100 mesh (c, d) and CM4-PSS sifting with 200 mesh (e, f).

observed, which is consistent with the highest mass gain (Table 1). When the morphologies of the CM2-PSS and CM3-PSS samples are compared, a more homogeneous surface can be seen, with smaller catalyst aggregates in the case of the CM3-PSS sample. The catalytic membrane prepared with catalyst particles smaller than $74\,\mu m$ (CM4-PSS) presented lower coverage at equal number of immersion-drying cycles than the CM3-PSS catalytic membrane. This could be due to the fact that the smaller particles employed to prepare the CM4-PSS could have less adhesion to the PdAu film than the larger ones employed for the CM3-PSS. On the surface image, a large region without catalyst covering can be seen, which shows the characteristic cauliflower-like morphology of the PdAu membranes. On the contrary, the regions of the CM3-PSS sample, which presented less agglomeration, are uniform covered with homogeneous particles of catalyst.

Also using SEM, top-view images of the Ru (CM7-PSS, Fig. 8a and b) and Rh (CM9-PSS, Fig. 8c and d) catalytic membranes were obtained. In these samples, the catalyst previously sieved with 100 mesh, was dispersed in ethanol and deposited on top of the PdAu membranes functionalized with a 1.0 v/v % APTES solution. Under the same synthesis conditions, the coating of the catalysts on the surface of both PdAu membranes was homogeneous, particles or agglomerates of similar size (up to $10\,\mu m$) being observed. It is possible to emphasize that the catalytic membranes prepared in this way, i.e. by functionalizing the surface with APTES prior to the deposition of the catalyst, show neither weight loss nor detachment after reduction at 823 K.

3.4. Catalytic evaluation

The catalytic results from the evaluation of the Ru and Rh powders in the DRM reaction, as well as those from the catalytic-based membranes are presented below. Table 3 shows the catalytic behavior of the $Ru(0.6\%)/La_2O_3(27\%)\text{-}SiO_2$ and $Rh(0.6\%)/La_2O_3(27\%)\text{-}SiO_2$ powders carried out in a FB reactor at 823 K. For both the Ru and Rh-based fresh catalysts (Ru-Fresh and Rh-Fresh samples, Table 3), conversion values were reached which correspond to the thermodynamic equilibrium under the analyzed conditions (W/F = $15.9 \times 10^{-6}\,g\,h\,mL^{-1}$, CH_4 and CO_2 equilibrium conversions at 823 K were 27% and 38%, respectively [32]). In this case, the H_2/CO ratios were lower than the unit, which indicates that the reverse water gas shift reaction also occurs. A lower methane conversion (ca. 8%) was obtained when the catalyst was evaluated after ethanol dispersion (Ru-EtOH sample, Table 3). This result could be related to a probable re-dissolution of Ru on ethanol and a consequent loss of the active phase. When the solid was treated on Ar at 573 K before the ethanol dispersion, a methane and a carbon dioxide conversion of ca. 22 and 29%, respectively, were obtained. These values are slightly lower than those obtained for the fresh catalyst (Table 3). For the $Rh(0.6\%)/La_2O_3(27\%)\text{-}SiO_2$ catalyst, similar CO_2 and CH_4 conversions were obtained on the fresh solid and after dispersion on ethanol (Rh-EtOH) (Table 3).

In order to study possible modifications in the $Ru/La_2O_3\text{-}SiO_2$ catalyst, XRF was employed to determine the compositions of the catalysts after they were submitted to different treatments. Such evaluated
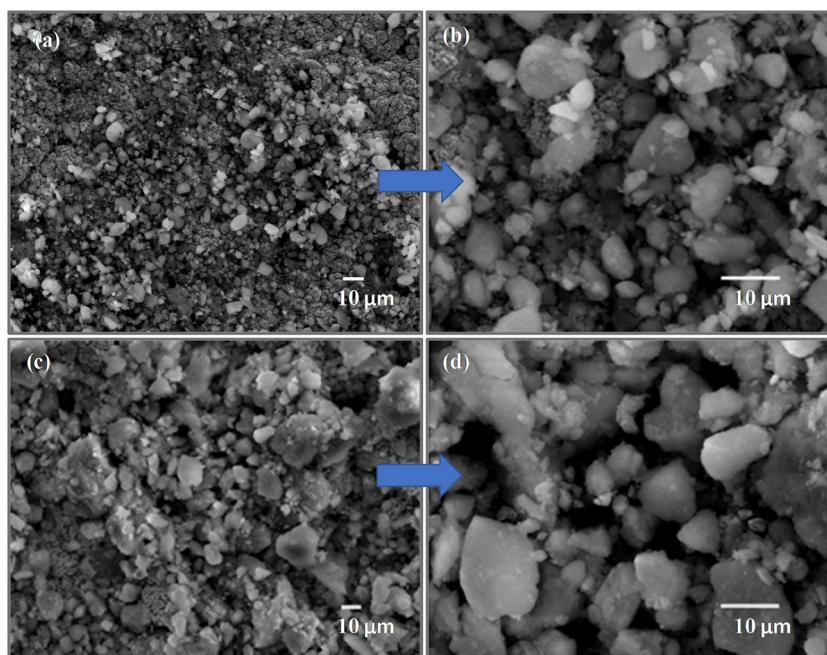
Fig. 8. Top surface view of the catalytic CM7-PSS (a, b) and CM8-PSS (c, d) membranes.

Table 3

Catalytic behavior of $Ru(0.6\%)/La_2O_3(27\%)-SiO_2$ and $Rh(0.6\%)/La_2O_3(27\%)-SiO_2$ catalysts powders at 823 K and W/F of 15.9×10^{-6} g h mL^{-1} in a fixed-bed reactor.

Sample	X_{CH_4}[a]	X_{CO_2}[a]	H_2/CO	Mol H_2 produced/ CH_4 feed ratio
Ru-Fresh[b]	25.4	31.8	0.69	0.53
Ru-EtOH[c]	8.1	18.2	0.35	0.08
Ru(Ar/573)[d]	22.2	29.4	0.53	0.32
Ru(Ar/573)-EtOH[e]	22.0	28.7	0.52	0.31
Rh-Fresh[f]	26.7	40.1	0.62	0.43
Rh-EtOH[g]	25.3	37.3	0.59	0.44

In all cases, the evaluated catalyst weight was 15 mg.

[a] Equilibrium CH_4 and CO_2 conversion at 823 K of 27% and 38%, respectively [34].

[b] $Ru(0.6\%)/La_2O_3(27\%)-SiO_2$ as synthesized catalyst.

[c] $Ru(0.6\%)/La_2O_3(27\%)-SiO_2$ catalyst without thermal treatment before its dispersion in anhydrous ethanol.

[d] $Ru(0.6\%)/La_2O_3(27\%)-SiO_2$ treated at 573 K in Ar flux for 2 h.

[e] $Ru(0.6\%)/La_2O_3(27\%)-SiO_2$ catalysts treated at 573 K in Ar flux for 2 h and dispersed in anhydrous ethanol.

[f] $Rh(0.6\%)/La_2O_3(27\%)-SiO_2$ after calcination at 823 K for 6 h.

[g] $Rh(0.6\%)/La_2O_3(27\%)-SiO_2$ after calcination at 823 K and dispersed in anhydrous ethanol.

variables were: i) fresh catalyst (Ru-Fresh), ii) fresh catalyst dispersed in anhydrous ethanol (Ru-EtOH), iii) catalyst treated in Ar at 573 K (Ru (Ar/573)) and iv) catalyst treated in Ar at 573 K followed by dispersion in ethanol (Ru(Ar/573)-EtOH). Table 4 summarizes the chemical composition of the catalysts after the different treatments. It can be observed that the Ru content in the catalyst decreased from 0.46 to 0.15% for the fresh and ethanol dispersed catalyst, respectively. Although the La_2O_3-SiO_2 support has been calcined at 823 K, a decrease in the lanthanum content from 31.6% up to 12.9% after the ethanol dispersion was observed. When a pretreatment in Ar atmosphere at 573 K was performed and afterwards the catalyst was dispersed in ethanol, the decrease in the Ru content was lower, with not change on the lanthanum content (Table 4). Considering this result, and also the unchanged catalytic activity of this solid, the former treatment was selected to prepare the Ru-based catalytic membranes.

Table 4

Composition of the catalysts after different treatments.

Sample	Thermal treatment	Ethanol	%SiO$_2$	%La$_2$O$_3$	%M[g]
Ru-Fresh[a]	No	No	67.8	31.6	0.46
Ru-EtOH[b]	No	Yes	86.9	12.9	0.15
Ru(Ar/573)[c]	Yes	No	66.8	32.6	0.46
Ru(Ar/573)-EtOH[d]	Yes	Yes	66.3	33.3	0.30
Rh-Fresh[e]	No	No	72.3	27.0	0.56
Rh-EtOH[f]	No	Yes	71.6	27.8	0.62

[a] $Ru(0.6\%)/La_2O_3(27\%)-SiO_2$ as synthesized catalyst.

[b] $Ru(0.6\%)/La_2O_3(27\%)-SiO_2$ catalyst without thermal treatment before its dispersion in anhydrous ethanol.

[c] $Ru(0.6\%)/La_2O_3(27\%)-SiO_2$ treated at 573 K in Ar flux for 2 h.

[d] $Ru(0.6\%)/La_2O_3(27\%)-SiO_2$ treated at 573 K in Ar flux for 2 h and dispersed in anhydrous ethanol.

[e] $Rh(0.6\%)/La_2O_3(27\%)-SiO_2$ after calcination at 823 K for 6 h.

[f] $Rh(0.6\%)/La_2O_3(27\%)-SiO_2$ after calcination at 823 K and dispersed in anhydrous ethanol.

[g] M refers to the Ru or Rh content.

A similar analysis scheme was performed for the Rh/La_2O_3-SiO_2 catalyst. In this case, fresh (Rh-Fresh) and dispersed in ethanol (Rh-EtOH) samples were evaluated. Clearly, no substantial differences in the chemical composition between both samples were observed. This difference in the behavior between the Ru and Rh based catalysts could be attributed to the fact that the former was calcined while the latter was not. This result suggests that the calcination process would stabilize the Rh, thus avoiding a re-dissolution of the active phase. In the case of the Ru catalyst, the calcination step was not carried out to avoid the formation of RuO_2 particles. Faroldi et al. [11] analyzed the activity and stability of Ru/La_2O_3-SiO_2 catalysts on the dry reforming of methane reaction, after different thermal treatments. The results showed that the catalysts calcined at 823 K presented lower reaction rate and stability than the uncalcined solid [11], probably related to an increase of the Ru particle size after treatment. Despite the pretreatment at 573 K in flowing Ar, the Ru-based catalyst behavior was more affected by being dispersed in anhydrous ethanol.

Table 5 summarizes the performance for the catalytic membranes and powder catalysts employing the same W/F (4.2×10^{-6} g h mL^{-1})

Table 5
Catalytic behavior for catalytic membranes and powder catalyst at 823 K and W/F of 4.2×10^{-6} g h mL^{-1}.

Sample	Catalyst	X_{CH_4}	X_{CO_2}	H_2/CO	%H$_2$ recovery[a]
CM2-PSS	Ru(0.6%)/La$_2$O$_3$(27%)-SiO$_2$[b]	5.3	5.5	0.96[c]	–
CM7-PSS	Ru(0.6%)/La$_2$O$_3$(27%)-SiO$_2$[b]	4.7	11.8	0.34[d]	38.6
CM9-PSS	Rh(0.6%)/La$_2$O$_3$(27%)-SiO$_2$[e]	5.3	12.9	0.59[c]	37.2
Ru(Ar/573)-EtOH	Ru(0.6%)/La$_2$O$_3$(27%)-SiO$_2$[b]	N.D.[f]	N.D.[f]	N.D.[f]	–
Rh-EtOh	Rh(0.6%)/La$_2$O$_3$(27%)-SiO$_2$[e]	4.8	10.1	0.29	–

[a] (H$_2$ permeated/H$_2$ produced)*100%.
[b] Ru(0.6%)/La$_2$O$_3$(27%)-SiO$_2$ catalysts treated at 573 K in Ar flux for 2 h and dispersed in anhydrous ethanol.
[c] Experimental value.
[d] Theoretical value.
[e] Rh(0.6%)/La$_2$O$_3$(27%)-SiO$_2$ catalysts after calcination at 823 K dispersed in anhydrous ethanol.
[f] N.D. means not detected.

at 823 K. The CM7-PSS and CM9-PSS samples exhibit similar mass gain and catalytic performance, even though the first was based on Ru and the second on Rh. As reported in the experimental section, the effective area of the catalytic membranes was ca. 0.5 cm^2, which resulted in ca. 4 mg of effective mass of catalyst being in contact with the reactants. Note that when the powdered catalyst was evaluated on the FB reactor using the same mass, a slightly smaller conversion was obtained for both catalysts, compared with the respective catalytic membranes (Table 3). Note that the equilibrium conversion was not reached in all cases when a W/F = 4.2×10^{-6} g h mL^{-1} was employed. For the CM2-PSS prepared with the Ru catalyst without thermal treatment, the methane and carbon dioxide conversions were similar, showing a H$_2$/CO ratio equal to 0.96. This could indicate that the reverse water gas shift reaction could be unfavored in this low Ru loading catalyst (Table 4). A hydrogen recovery factor (H$_2$ permeated/H$_2$ produced) of ca. 38% was obtained with the catalytic membranes under the operation conditions selected in this study (Table 5). Using a Pd tubular membrane, coupled with a Rh(0.6%)/La$_2$O$_3$ catalyst, Bosko et al. [9] reported a hydrogen recovery of about 30% for a sweep gas flow rate of 10 mL min^{-1} at 773 K, a W/F = 2.4×10^{-3} g h mL^{-1} and a higher permeation area (7.3 cm^2). Most studies reported in the literature focusing on methane dry reforming in Pd membrane reactors use an extractor type configuration, where hydrogen is extracted from the reaction zone with the consequent increase in conversion [12,32–34]. However, so far, no data has been reported using MRs where the selective layer and the catalyst are integrated in the same substrate.

The catalytic membranes developed for hydrogen production were mainly prepared by deposition of the catalyst on the porous structure of the support and coupling the Pd or Pd-alloy layer on the other side [13–16]. Few studies have reported the coating of the catalyst on top of the selective layer with an approach similar to that used in our case [34,35]. By co-sputtering Pt and CeO$_2$ over a thin PdAu composite membrane of 19.6 cm^2, Park and coworkers [34] developed a bi-functional membrane which enhance the performance of the WGS reaction. With a catalyst layer of 2.6 μm thick, and a ΔP of 500 kPa, the CO conversion was twice of that obtained when not hydrogen permeation across the membrane occurs.

Although the conversions reached with the CMs prepared in this work were low, they were higher or similar to those obtained with the powdered catalysts under the same conditions. It is important to note that the evaluations were made employing a low mass of catalyst, in addition to the use of catalysts which have a low percentage of active

phase (ruthenium or rhodium). Nevertheless, from these preliminary results, it should be noted that it will be possible to obtain hydrogen with a high degree of purity due to the high selectivity of the PdAu membrane. Greater efforts are being made to optimize the amount of catalyst deposition on the membrane surface and increase the permeation area.

4. Conclusions

Successful APTES functionalizations of PdAu surfaces were performed. The increase in APTES concentration led to an increase in the Si/Pd and N/Pd surface ratio. When an APTES concentration of 0.5 v/v % was employed, a surface saturation was reached while Si/Pd and N/Pd volumetric ratio remained approximately constant in all samples.

Grafted samples proved to be stable against heat treatment up to 823 K for 2 h. A conservation of the perm-selective characteristics of the PdAu membranes after functionalization with APTES was also observed.

Catalytic Ru an Rh-based membranes were evaluated on the dry reforming of methane at 823 K. They showed similar conversions values when they were compared to the data obtained with powder samples in a fixed-bed reactor under the same conditions. Despite the low conversions values, these results are very promising for obtaining high purity H$_2$. Greater efforts are being made to optimize and improve the catalyst deposition on the membrane surface and thus increase the mass gain.

References

[1] G. Di Marcoberardino, M. Binotti, G. Manzolini, J.L. Viviente, A. Arratibel, L. Roses, F. Gallucci, Achievements of European projects on membrane reactor for hydrogen production, J. Clean. Prod. 161 (2017) 1442–1450.
[2] F. Bilgili, E. Koçak, Ü. Bulut, The dynamic impact of renewable energy consumption on CO$_2$ emissions: a revisited environmental Kuznets curve approach, Renew. Sustain. Energy Rev. 54 (2016) 838–845.
[3] M.R. Rahimpour, M. Bayat, Production of ultrapure hydrogen via utilizing fluidization concept from coupling of methanol and benzene synthesis in a hydrogen-permselective membrane reactor, Int. J. Hydrogen Energy 36 (2011) 6616–6627.
[4] A. Hedayati, O. Le Corre, B. Lacarrière, J. Llorca, Dynamic simulation of pure hydrogen production via ethanol steam reforming in a catalytic membrane reactor, Energy 117 (2016) 316–324.
[5] D. Mendes, V. Chibante, J.-M. Zheng, S. Tosti, F. Borgognoni, A. Mendes, L.M. Madeira, Enhancing the production of hydrogen via water-gas shift reaction using Pd-based membrane reactors, Int. J. Hydrogen Energy 35 (2010) 12596–12608.
[6] S. Arora, R. Prasad, An overview on dry reforming of methane: strategies to reduce carbonaceous deactivation of catalysts, RSC Adv. 6 (2016) 108668–108688.
[7] J.M. Leimert, J. Karl, M. Dillig, Dry reforming of methane using a nickel membrane reactor, Processes 5 (2017) 82–95.
[8] F. Gallucci, E. Fernandez, P. Corengia, M. van Sint Annaland, Recent advances on membranes and membrane reactors for hydrogen production, Chem. Eng. Sci. 92 (2013) 40–66.
[9] M.L. Bosko, J.F. Múnera, E.A. Lombardo, L.M. Cornaglia, Dry reforming of methane in membrane reactors using Pd and Pd-Ag composite membranes on a NaA zeolite modified porous stainless steel support, J. Membr. Sci. 364 (2010) 17–26.
[10] T.A. Peters, M. Stange, H. Klette, R. Bredesen, High pressure performance of thin Pd-23%Ag/stainless steel composite membranes in water gas shift gas mixtures; influence of dilution, mass transfer and surface effects on the hydrogen flux, J. Membr. Sci. 316 (2008) 119–127.
[11] B.M. Faroldi, E.A. Lombardo, L.M. Cornaglia, Surface properties and catalytic behavior of Ru supported on composite La$_2$O$_3$-SiO$_2$ oxides, Appl. Catal. A 369 (2009) 15–26.
[12] B.M. Faroldi, E.A. Lombardo, L.M. Cornaglia, Ru/La$_2$O$_3$-SiO$_2$ catalysts for hydrogen production in membrane reactors, Catal. Today 172 (2011) 209–217.
[13] T. Maneerung, K. Hidajat, S. Kawi, Triple-layer catalytic hollow fiber membrane reactor for hydrogen production, J. Membr. Sci. 514 (2016) 1–14.

[14] N. Prasetyaa, Z. Wu, A.G. Gila, K. Li, Compact hollow fiber reactors for efficient methane conversion, J. Eur. Ceram. Soc. 37 (2017) 5281–5287.

[15] F.R. García-García, L. Torrente-Murciano, D. Chadwick, K. Li, Hollow fiber membrane reactors for high H_2 yields in the WGS reaction, J. Membr. Sci. 405–406 (2012) 30–37.

[16] F.R. García-García, M.A. Rahman, I.D. González-Jiménez, K. Li, Catalytic hollow fiber membrane micro-reactor: high purity H_2 production by WGS reaction, Catal. Today 171 (2011) 281–289.

[17] A.M. Tarditi, C. Gerboni, L.M. Cornaglia, PdAu membranes supported on top of vacuum-assisted ZrO_2-modified porous stainless steel substrates, J. Membr. Sci. 428 (2013) 1–10.

[18] A.M. Tarditi, F. Braun, L.M. Cornaglia, Novel PdAgCu ternary alloy: hydrogen permeation and surface properties, Appl. Surf. Sci. 257 (2011) 6626–6635.

[19] J. Kunze, A. Ghicov, H. Hildebrand, J.M. Macak, L. Traveira, P. Schmuki, Challenges in the surface analytical characterization of anodic TiO_2 films-a review, Z. Phys. Chem. 219 (2005) 1561–1582.

[20] J. Zheng, Z. Zhu, H. Chen, Z. Liu, Nanopatterned assembling of colloidal gold nanoparticles on silicon, Langmuir 16 (2000) 4409–4412.

[21] S. Yang, P. Yuan, H. He, Z. Qin, Q. Zhou, J. Zhu, D. Liu, Effect of reaction temperature on grafting of γ-aminopropyl triethoxysilane (APTES) onto kaolinite, Appl. Clay Sci. 62–63 (2012) 8–14.

[22] H.J. Song, N. Li, Y. Li, C. Min, Z. Wang, Preparation and tribological properties of graphene/poly(ether ether ketone) nanocomposites, J. Mater. Sci. 47 (2012) 6436–6443.

[23] N. Majoul, S. Aouida, B. Bessaïs, Progress of porous silicon APTES-functionalization by FTIR investigations, Appl. Surf. Sci. 331 (2015) 388–391.

[24] K.M. Parida, R. Dharitri, Amine functionalized MCM-41: an active and reusable catalyst for Knoevenagel condensation reaction, J. Mol. Catal. A Chem. 310 (2009) 93–100.

[25] E. Vunain, N.N. Opembe, K. Jalama, A.K. Mishra, R. Meijboom, Thermal stability of amine-functionalized MCM-41 in different atmospheres, J. Therm. Anal. Calorim.

115 (2014) 1487–1496.

[26] P. Chen, G. Deng, D. Hu, Y. Wang, Z. Meng, W. Hua, K. Xi, Enhanced mechanical properties and thermal stability of PSMA by functionalized graphene nanosheets, RSC Adv. 6 (2016) 68748–68753.

[27] F.A. Lewis, Palladium Hydrogen System, Academic Press, London and New York, 1967.

[28] S. Yun, S.T. Oyama, Correlations in palladium membranes for hydrogen separation: a review, J. Membr. Sci. 375 (2011) 28–45.

[29] A. Huang, F. Liang, F. Steinbach, J. Caro, Preparation and separation properties of LTA membranes by using 3-aminopropyltriethoxysilane as covalent linker, J. Membr. Sci. 350 (2010) 5–9.

[30] A. Huang, W. Dou, J. Caro, Steam-stable zeolitic imidazolate framework ZIF-90 membrane with hydrogen selectivity through covalent functionalization, J. Am. Chem. Soc. 132 (2010) 15562–15564.

[31] Y. Martínez Galeano, L. Cornaglia, A.M. Tarditi, NaA zeolite membranes synthesized on top of APTES-modified porous stainless steel substrates, J. Membr. Sci. 512 (2016) 93–103.

[32] F.A. Silva, C.E. Hori, A.M. Da Silva, L.V. Mattos, J. Múnera, L. Cornaglia, F.B. Noronha, E. Lombardo, Hydrogen production through CO_2 reforming of CH_4 over $Pt/CeZrO_2/Al_2O_3$ catalysts using a Pd-Ag membrane reactor, Catal. Today 193 (2012) 64–73.

[33] S. Irusta, J. Múnera, C. Carrara, E.A. Lombardo, L.M. Cornaglia, A stable, novel catalyst improves hydrogen production in a membrane reactor, Appl. Catal. A 287 (2005) 147–158.

[34] K.-R. Hwang, S.-W. Lee, D.-W. Lee, C.-B. Lee, S.-M. Ji, J.-S. Park, Bi-functional hydrogen membrane for simultaneous chemical reaction and hydrogen separation, Int. J. Hydrogen Energy 39 (2014) 2614–2620.

[35] D. Kim, K. Barnett, B.A. Wilhite, Experimental demonstration of enhanced hydrogen permeation in palladium via a composite catalytic-permselective membrane, AIChE J. 59 (2013) 1627–1634.